Article

Cell Reports

The Integration of Goal-Directed Signals onto Spatial Maps of Hippocampal Place Cells

Graphical Abstract

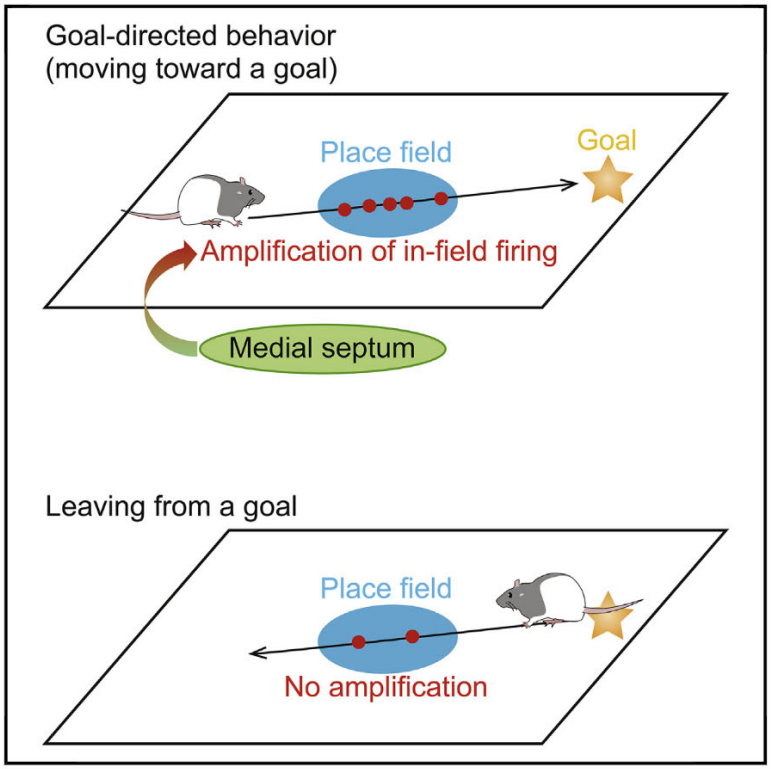

Authors

Yuki Aoki, Hideyoshi Igata, Yuji Ikegaya, Takuya Sasaki

Correspondence

tsasaki@mol.f.u-tokyo.ac.jp

In Brief

Aoki et al. find that firing rates of CA1 neurons increase when rats are running toward a goal location irrespective of the positional relationship between their place fields and goal location. The results suggest possible neurophysiological mechanisms for encoding place-selective and goal-directed signals by a hippocampal cell.

Highlights

- In-field firing rates of hippocampal cells increase during goal-directed behavior
- Internally motivated goal-directed behavior boosts in-field firing
- Medial septal inactivation reduces goal-directed firing

Aoki et al., 2019, Cell Reports 27, 1516–1527
April 30, 2019
https://doi.org/10.1016/j.celrep.2019.04.002

CellPress

OPEN ACCESS
CellPress

Cell Reports
Article

The Integration of Goal-Directed Signals onto Spatial Maps of Hippocampal Place Cells

Yuki Aoki,[1] Hideyoshi Igata,[1] Yuji Ikegaya,[1,2] and Takuya Sasaki[1,3,4,*]
[1]Graduate School of Pharmaceutical Sciences, The University of Tokyo, 7-3-1 Hongo, Bunkyo-ku, Tokyo 113-0033, Japan
[2]Center for Information and Neural Networks, 1-4 Yamadaoka, Suita City, Osaka 565-0871, Japan
[3]Precursory Research for Embryonic Science and Technology (PRESTO), Japan Science and Technology Agency (JST), 4-1-8 Honcho, Kawaguchi, Saitama 332-0012, Japan
[4]Lead Contact
*Correspondence: tsasaki@mol.f.u-tokyo.ac.jp
https://doi.org/10.1016/j.celrep.2019.04.002

SUMMARY

Spatial firing of hippocampal place cells varies depending on the animal's behavior relative to its goals. Here, rats were trained to approach visually guided reward ports in a two-dimensional open field. Hippocampal place cells encoded two independent pieces of information, spatial representation and goal-directed representation, by amplifying firing rates within their place fields specifically while the animal was moving toward a specific goal location. Irrespective of running speed and direction, substantial place-selective firing was observed that sustained a basal spatial map independent of goal-directed signals. When animals were allowed to freely forage in the field, in-field firing rates similarly increased when the animals transiently ran toward remembered goal locations. Disruption of medial septal activity significantly decreased goal-directed firing while maintaining spatial representation patterns. The findings indicate that the integrated encoding of spatial and goal-directed signals by hippocampal circuits is crucial for flexible spatial navigation to a goal location.

INTRODUCTION

Hippocampal place cells fire when an animal visits a restricted area of an environment (O'Keefe and Dostrovsky, 1971) and have been suggested to constitute a cognitive map of an animal's spatial locations (O'Keefe and Nadel, 1978). A widely used behavioral task for characterizing place cell firing is a random foraging task in which rodent animals freely explore a two-dimensional field in search of randomly dispersed food scraps. In tasks without any goal locations, place cell spikes within their place fields emerge with little dependence on moving direction (Muller et al., 1994).

A recent study by Aghajan et al. (2015) demonstrated that hippocampal neurons with no spatial selectivity during random foraging in two-dimensional virtual reality emitted place-selective firing after animals switched their behavioral patterns from random movement to running toward a reward location in the same space. This observation suggests that spatial selectivity of hippocampal cells is strongly determined by goal-directed behavior. The presence of a conjunctive representation of goal-directed behavior and space in single hippocampal neurons raises an intriguing issue of how spatial and goal-directed signals are integrated and processed in the hippocampus. Here, goal-directed firing refers to the firing of hippocampal cells observed during movement toward goals, which is distinct from goal-related firing observed during almost stopping at a location (Hok et al., 2007).

A number of studies have shown that hippocampal cell firing within their place fields (termed in-field firing) highly differs when animals pass through an identical space. For example, hippocampal cells specifically increase their in-field firing rates during running toward a given direction, but not in the opposite direction, along a linear path such as a linear track, a W-shaped track, or a radial maze (McNaughton et al., 1983; Frank et al., 2000; Jackson and Redish, 2007; Yagi et al., 2018). Similar directional firing patterns have been found in hippocampal neurons of bats flying in a three-dimensional open space (Sarel et al., 2017). As a running direction in these studies corresponds with a direction toward a goal, it is difficult to determine whether such direction-dependent firing represents an absolute running direction or one of several possible directions toward a specific goal. In T-shaped and plus-shaped mazes where animals have to take either a left or a right route at a branch point, in-field firing rates of hippocampal cells are highly differentiated depending on future trajectories, so-called splitter cells (Wood et al., 2000; Ferbinteanu and Shapiro, 2003; Ji and Wilson, 2007; Catanese et al., 2014; Ito et al., 2015; Takahashi, 2015). Similar trajectory-dependent firing patterns have been observed from mazes with multiple choice points (Ainge et al., 2007; Grieves et al., 2016). As such trajectory-dependent firing patterns were recorded when animals ran in only one direction on a linear path, it is difficult to determine whether they represent a particular trajectory or one of many trajectories for a goal.

To answer these questions, we constructed a cued task in which animals move toward multiple reward locations signaled by visual cues in a two-dimensional space. Enhancing the degree of freedom of moving directions from multiple start points to multiple goal points allowed us to analyze how in-field firing patterns vary when animals pass through their place fields from multiple inbound and outbound directions. After the cued task, the animals freely foraged for randomly dispersed food in the same field. In this condition, animals did not just perform

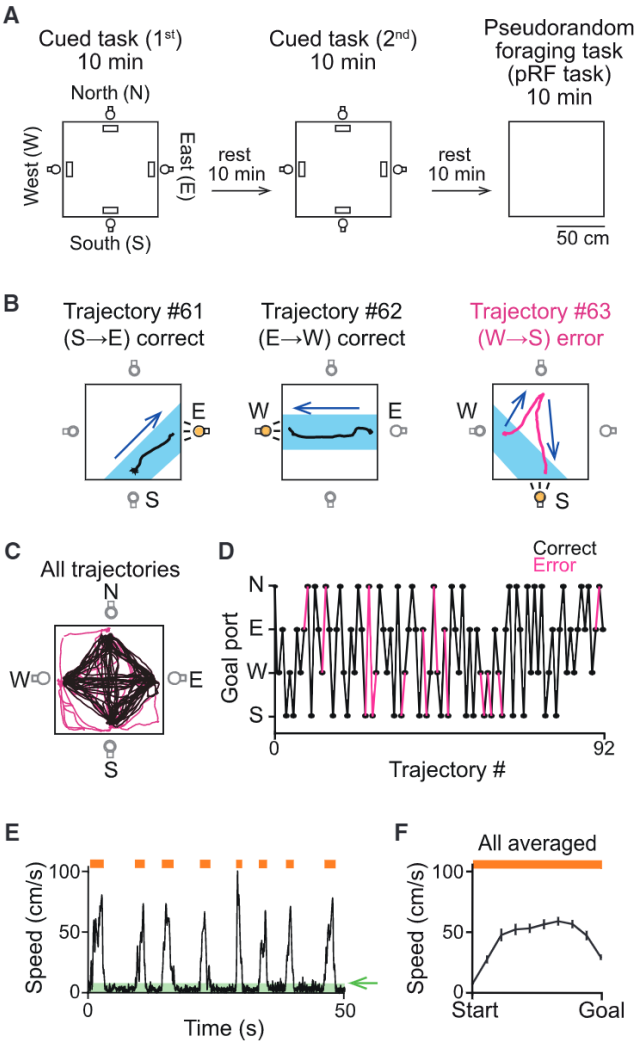

Figure 1. Behavioral Patterns in a Cued Task

(A) A schematic illustration of the experimental paradigm. On a recording day, rats performed two 10-min sessions of a cued task followed by a 10-min session of a pseudorandom foraging (pRF) task. Both tasks were tested in an identical 1-m^2 open field. Each session was flanked by a 10-min rest session.

(B) Representative three sequential trajectories in the cued task. In each journey, a cue light was illuminated (colored in yellow), indicating that the corresponding port provided a reward. A trajectory was defined as an error trajectory if the animal ran outside of the cyan region (e.g., trajectory 63).

(C) All trajectories in a 10-min cued task were superimposed (black, correct; magenta, error).

(D) All journeys shown in (C) are represented as lines from a start port to a goal port (black, correct; magenta, error).

(E) Representative running speed of an animal during a 50-s period in the cued task. Periods of running and reward consumption are typically represented as transient increases in speed and a speed less than 10 cm/s (green-shaded area), respectively.

(F) Average temporal changes in running speed from a reward port to the next one (n = 1,080 trajectories from seven animals). Each period for each journey was normalized in time.

See also Figure S1.

random foraging behavior but occasionally exhibited transient running toward previous reward locations, which allowed us to analyze how firing patterns of the same cells were affected by internally motivated behavior. Finally, we tested the contribution of medial septal activity to goal-directed and spatial firing by acute inhibition of the medial septum.

RESULTS

A Cued Task in an Open Field

A total of 11 rats were tested with a sequence of two behavioral tasks, a cued task and a pseudorandom foraging (pRF) task. In the cued task, four reward ports were placed on the floor of a two-dimensional open field, and light-emitting diodes (LEDs) were attached to walls above the individual reward ports (Figure 1A). A randomly assigned reward port provided a chocolate milk reward, and the LED above the port was illuminated as a visual cue. Once the rat started to consume the reward, the current cue signal was turned off, and the next randomly chosen port was baited together with the illumination of the LED above the port. Before electrode implantation surgery, rats were trained on the task for 10.0 ± 2.0 days until they reached a behavioral criterion that consisted of consuming the reward at least 40 times within a 10-min session of the cued task (n = 11 rats). Representative running trajectories from a reward port to the next port from a well-trained rat are shown in Figures 1B and 1C. Each trajectory was classified as a correct or an error trajectory (Figure 1D; see STAR Methods), and only correct trajectories were used for all analyses. On average, a well-trained rat completed 42.0 ± 4.3 correct trajectories out of 46.0 ± 5.1 total trajectories (n = 18 days from 11 rats). A representative running speed of a rat during a single 10-min session of the cued task is shown in Figure 1E. The average peak running speed from one port to the next was 69.5 ± 2.4 cm/s (Figure 1F; n = 1,023 trajectories from 11 rats). No significant differences in running speed were found between a given journey (going toward a port) and the opposite journey (leaving from the port) for all twelve journey patterns (Figure S1).

Goal-Directed Spiking Activity in the Cued Task

Spike patterns in the cued task were recorded from a total of 183 hippocampal CA1 neurons from 11 rats. Figure 2A summarizes the firing patterns of a representative goal-directed cell, with each panel showing journey patterns toward one of four reward ports with three different directions in the cued task. For each journey, spike locations were projected onto a line between the start and goal ports, and the average firing-rate distribution along the projected line was computed (Figure 2A, right). A repeated-measures ANOVA was performed to assess the significant differences in average firing-rate distributions associated with two journeys in opposite directions on the same projection line. For the example cell in Figure 2A, the firing-rate distributions associated with three journeys toward port E were significantly higher than those associated with the three opposite journeys leaving port east (E) ($p_{group} < 0.01$ for north-to-east [NE] versus EN journeys, west-to-east [WE] versus EW journeys, and south-to-east [SE] versus ES journeys), defining this cell as a goal-directed cell, port E as a goal location, and NE, WE, and

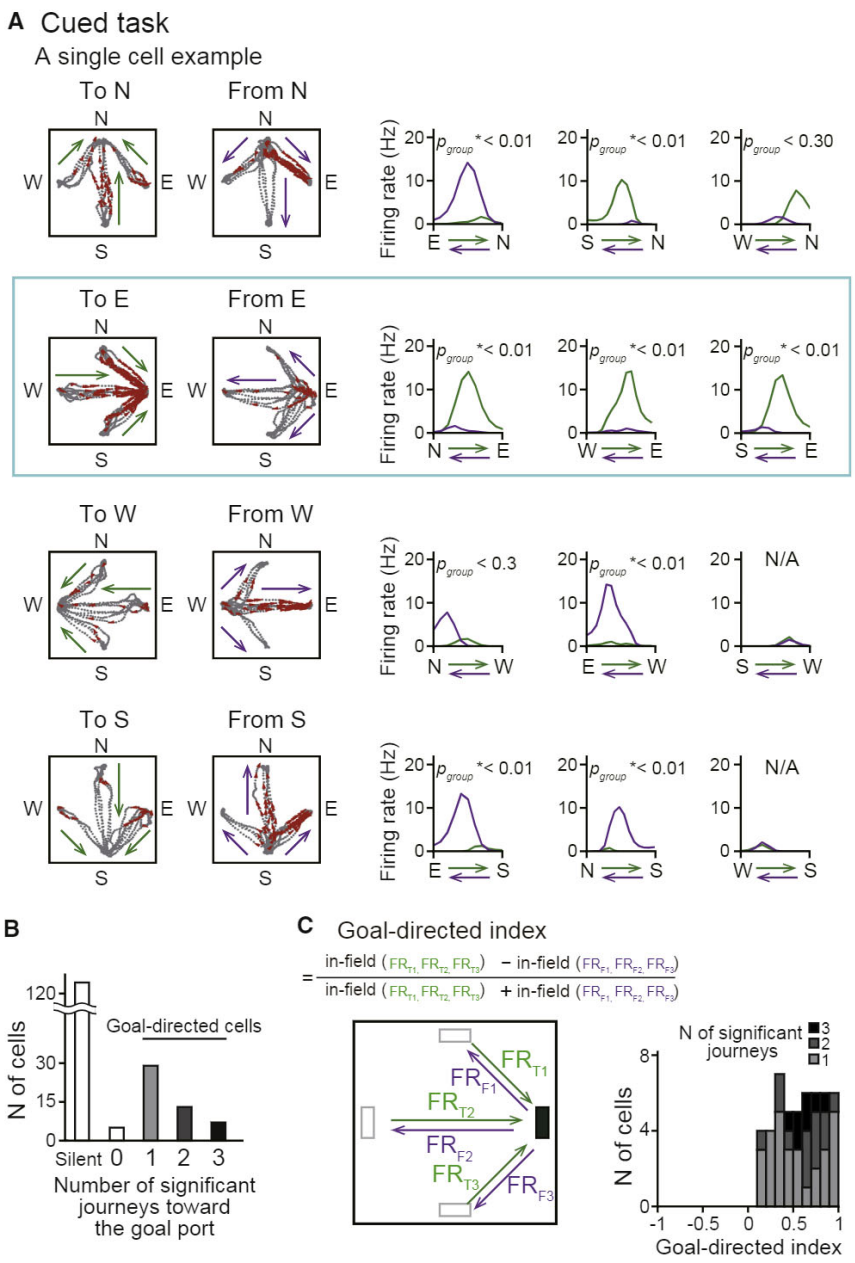

Figure 2. Goal-Directed Firing toward a Reward Port in the Cued Task

(A) Firing patterns of a representative single hippocampal cell. The left two panels show the superimposed trajectories of three journeys approaching and leaving a specific port during a 10-min session. Positions of spikes are represented as colored dots superimposed on position samples of trajectories (gray dots). Spikes emitted at a running speed of <10 cm/s were excluded from these graphs. The green and purple arrows indicate journey directions. The right three panels show average firing-rate distributions computed from the individual journey patterns shown in the left two panels. In each panel, a two-way ANOVA was conducted to assess the significance of the difference (p_{group}) in firing-rate distributions between two opposite journeys. Panels with maximum firing rates less than 2 Hz in both firing-rate distributions were not analyzed (labeled as N/A). For this representative cell, three significant journeys approaching port E had $p_{group} < 0.01$, defining port E as the goal port (cyan box).

(B) For each cell, the number of significant journeys with $p_{group} < 0.01$ toward a goal port. Cells that had firing rates of less than 2 Hz and were not analyzed by two-way ANOVAs were classified as silent.

(C) (Left) Schematic illustration showing how the goal-directed index for a cell to a goal port represented by the black box is computed, where in-field firing rates in significant journeys toward and away from the goal port (black box) are FR_{T1}, FR_{T2}, and FR_{T3}, and FR_{F1}, FR_{F2}, and FR_{F3}, respectively. (Right) Distribution of goal-directed indexes of all goal-directed cells. Each color shows the number of significant journeys, corresponding with (B). See also Figures S2 and S3.

SE journeys as significant journeys for this cell (see STAR Methods; other example cells are shown in Figure S2). Out of 183 cells tested, 49 cells were classified as goal-directed cells that have at least one significant journey. The numbers of significant journeys ranged from one to three, which are summarized in Figures 2B and 2C. The variance of the number of significant journeys was mainly due to the locations of individual place fields in relation to goal ports; one significant journey tended to be detected from a larger proportion of goal-directed cells with their place fields located near a start port or at the middle of a journey, whereas three significant journeys tended to be detected from a larger proportion of goal-directed cells with their place fields located near a goal port (Figure 3D). For each goal-directed cell, a goal-directed index was computed that quantified the degree of biased in-field firing toward a goal port, as shown in Figure 2C.

An alternative explanation for the goal-directed firing may be that it is correlated with an animal's head direction (Taube et al., 1990), though it has been reported that hippocampal place cells exhibit little dependence on head direction (Muller et al., 1994). To address this issue, for each goal-directed cell, polar plots were constructed in which firing rates were plotted against goal-oriented moving directions or head directions (Figures S3A and S3B). Based on the polar plots, the mean vector length for goal-oriented moving directions and head directions (MVL_{goal} and MVL_{head}) were compared in goal-directed cells having three significant journeys (Figure S3C). Overall, MVL_{goal} was significantly higher than MVL_{head} ($t_6 = 9.58$, $p = 7.4 \times 10^{-5}$), demonstrating that firing-rate changes of these cells were more strongly tuned to goal-oriented moving directions. To further validate this idea, firing rates in each goal-directed cell were compared between a

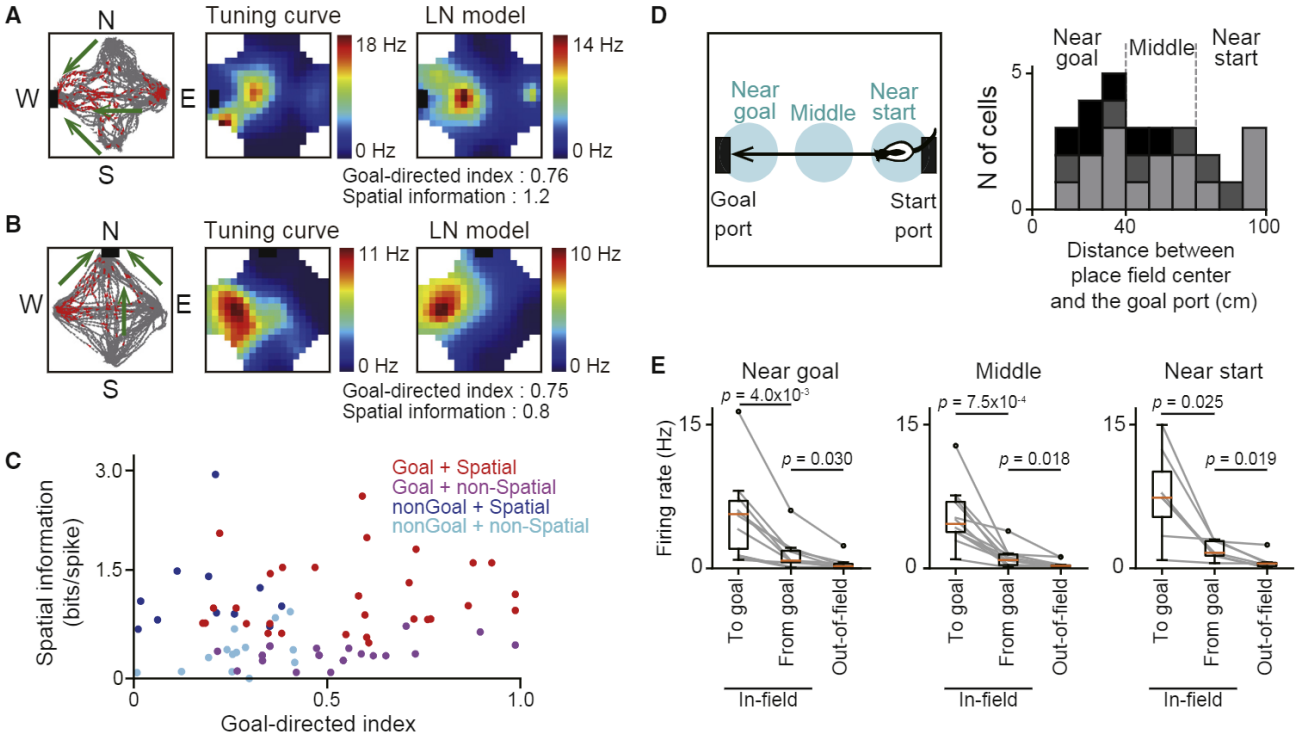

Figure 3. Goal-Directed Behavior Determines the Place-Selective Firing of Hippocampal Cells

(A and B) Firing patterns of two representative cells in the cued task. Cells with their goal ports at west (A) and north (B) are shown. (Left) All trajectories (gray) and spike locations (red) in the cued task were superimposed. The green arrows represent significant journeys to a reward port (black box). (Middle) All spatial firing patterns were converted into a conventional color-coded firing-rate map (tuning curve) with a color scale from 0 Hz (blue) to the peak rate (red). (Right) The tuning curve-based spatial map was converted into a different color-coded firing-rate map by the LN model proposed by Hardcastle et al. (2017). Spatial information was computed based on the LN model-based color map (other example cells are shown in Figure S1).

(C) Summarized plots showing the relationship between spatial information and the goal-directed index. Each dot represents each cell based on cell types.

(D) (Left) Schematic images of classification of place fields relative to goal ports. Reward ports and individual types of place fields are shown by the black boxes and cyan-filled circles, respectively. Place fields with distances <40, 40–70, and >70 cm from their goal ports were classified as near goal, middle, and near start fields, respectively. (Right) Distribution of the distance between a goal port and a place field center for each goal-directed spatial cell. Each color shows the number of significant journeys, corresponding with Figure 2B.

(E) Significant journeys crossing the place field during running toward and from the goal port are termed "to goal" and "from goal," respectively. For each cell, in-field firing rates were separately computed for directions of "to goal" and "from goal" (near goal, n = 12 cells; middle, n = 9 cells; near start, n = 6 cells). Out-of-field firing rates were classified as "out of field." Paired t test followed by Bonferroni correction.

See also Figure S4.

given significant journey and the other journey that is parallel to the significant journey with the same head direction (Figures S3D and S3E). The differences in firing rates on the two journeys were quantified by computing p_{group}, the same as in Figure 2A. In all goal-directed cells tested, p_{group} was less than 0.05 (Figure S3F). The ratio of the difference between two firing rates to the sum of the two firing rates, termed a FR ratio, was 0.72 ± 0.03 (Figure S3G). These results suggest that firing-rate increases in the cued task are more strongly determined by goal-oriented moving directions rather than head directions.

Spatial Firing of Hippocampal Cells Depends on Goal-Directed Behavior

The majority of goal-directed cells exhibited spatially selective spikes (two examples are shown in Figures 3A and 3B). For each cell, a spatial firing-rate map was first constructed as a tuning curve, similar to a general place cell analysis. As shown in Figure 1F, running speed in the cued task varied depending on position, meaning that the time spent in each location bin differed considerably. The linear-nonlinear-Poisson (LN) model was thus applied to the tuning curve-based spatial maps to compensate for running speed differences across locations (for details, see Hardcastle et al., 2017; LN model). From the LN model-based spatial maps, spatial information was computed for each cell to define the spatial selectivity (for details, see the STAR Methods). The relationship between spatial information and goal-directed indexes for all active cells tested is summarized in Figure 3C. Out of 183 cells tested, 21.9% (40 cells) were classified as spatial cells, and 15.8% (29 cells) were classified as goal-directed spatial cells. To examine the positional relationship between place field locations and goal directionality, the distance between the place field center and the goal port was computed for each goal-directed spatial cell, and place fields with distances <40, 40–70, and >70 cm were classified as

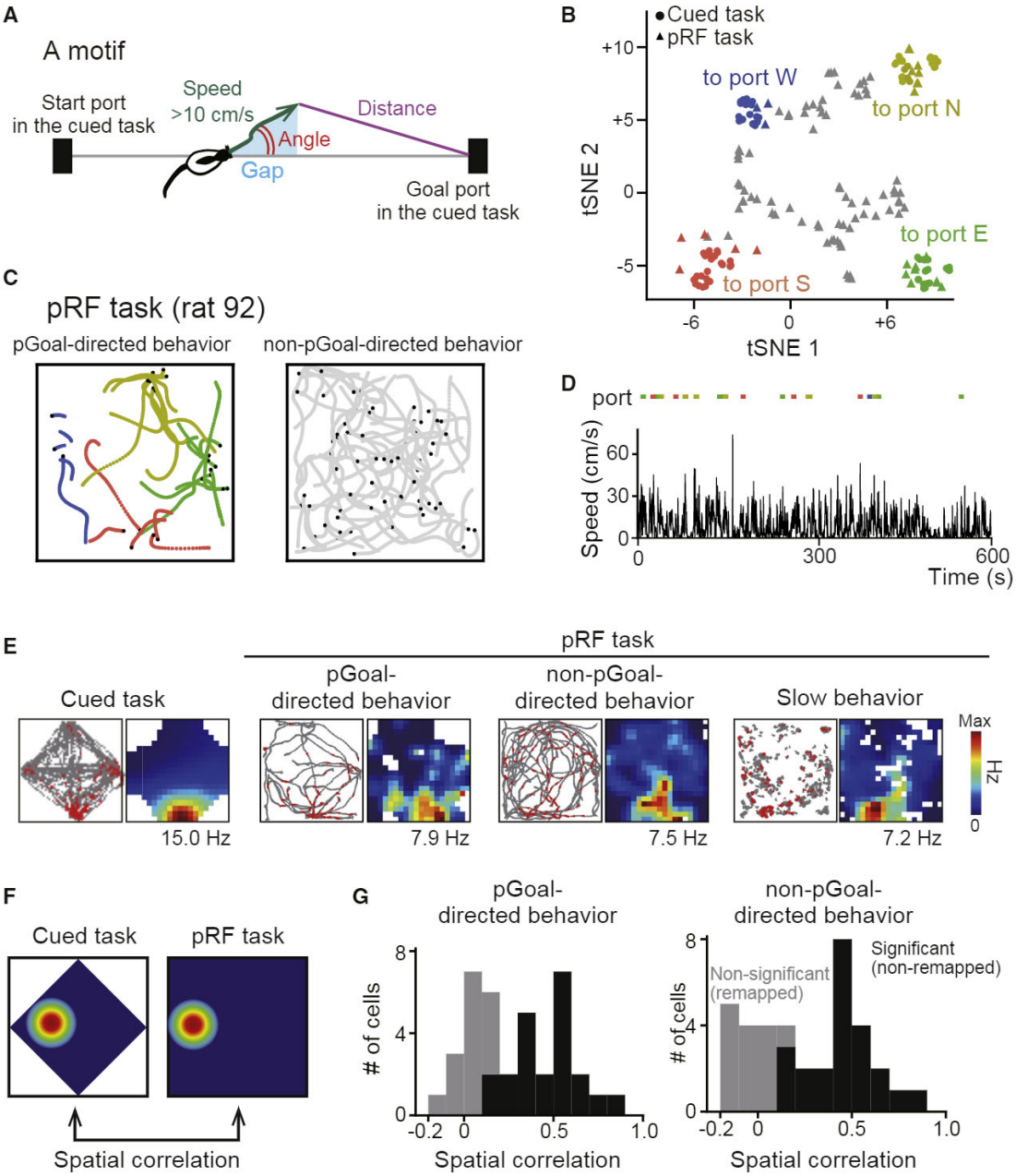

Figure 4. Spatial Firing Patterns in the pRF Task

(A) For each moving motif with a running speed >10 cm/s, the angle (red), distance (magenta), and gap (cyan) for individual goal ports were computed. The gray line is a straight line between start and goal ports.

(B) The three factors were computed for individual goal ports, resulting in a twelve-dimensional vector for a motif. The vectors from a single rat were decomposed into two-dimensional vectors by t-SNE (colored circle, cued task; triangle, pRF task). Motifs classified as pGoal-directed behavior in the pRF task from a single rat were labeled in different colors according to goal ports toward which the rats ran, whereas the other motifs were classified as non-pGoal-directed behavior (gray triangles).

(C) Trajectories with pGoal-directed behavior (left) and non-pGoal-directed behavior (right) in the pRF task in the rat. Trajectories toward the different ports are shown in different colors, corresponding with (B). The black dots indicate the last points of individual motifs.

(D) Rat running speed corresponding with (C). Periods of pGoal-directed behavior toward goal ports are indicated by the colored dots above.

(E) Comparison of spatial firing patterns of a representative cell among the cued task, pGoal-directed behavior, non-pGoal-directed behavior, and slow behavior in the pRF task, shown as in Figure 3A. The maximum firing rate in each map is shown below.

(F) Spatial correlation coefficients were computed between two firing-rate maps of the cued task and individual periods of the pRF task.

(legend continued on next page)

near goal, middle, and near start fields, respectively (Figure 3D). The presence of the middle and near start fields demonstrates that place fields did not always emerge at goal locations in some cell populations. In this study, it is impossible to determine whether near-goal place fields represent true place fields independent of reward signals or if they were a part of neuronal representations of reward-predictive signals (Gauthier and Tank, 2018). For all types of place fields, in-field firing rates during moving toward goal ports ("to goal") were significantly higher than those during departing from goal ports ("from goal") (Figure 3E; near goal, $t_{11} = 3.52$, $p = 0.025$; middle, $t_8 = 5.04$, $p = 7.5 \times 10^{-4}$; near start, $t_5 = 4.29$, $p = 0.0040$), confirming that in-field firing rates prominently increased while the rat ran toward a goal port. Notably, in-field firing rates during the rat's departure from the goal ports were still significantly higher than out-of-field firing rates averaged over all periods (Figure 3E; near goal, $t_{11} = 3.76$, $p = 0.019$; middle, $t_8 = 3.16$, $p = 0.018$; near start, $t_5 = 2.99$, $p = 0.030$). Taken together, these results suggest that hippocampal cells receive constant place-selective excitatory drives within their place fields that sustain in-field firing, irrespective of goal-related directions, and such excitatory drives are specifically amplified by goal-related behavior to boost in-field firing rates.

There is a possibility that self-localization of an animal's head direction toward the next goal port, termed goal-oriented behavior, may be sufficient to evoke the boosting of in-field firing rates. To test this idea, in-field firing rates of goal-directed cells with their place fields located near start ports were specifically analyzed by plotting moment-to-moment goal-oriented head directions (Figure S4A). The plot showed that in-field firing rates began to significantly increase when goal-oriented head directions were less than 30°, compared with those at 180°–90° (Figure S4B). Furthermore, the goal-pointing onset-triggered average of firing rates showed that firing rates started to increase just when an animal oriented its head toward the next goal port (Figure S4C). These results suggest that pointing an animal's head direction toward the goal port evokes goal-directed firing of place cells.

Behavioral Patterns in the pRF Task

Following the cued task, all goal ports and light cues were removed, and the rats were then allowed to freely explore the same field for 10 min to obtain randomly scattered chocolate milk (Figure 4). In this foraging task, the rats occasionally exhibited running behavior similar to that observed in the cued task as if they expected the presence of reward ports that were no longer present, termed as pseudo-goal-directed (pGoal-directed) behavior. Therefore, this foraging task was termed the pRF task. To define pGoal-directed behavior, a portion of a trajectory with running speed >10 cm/s was extracted as a moving motif. Other behavioral patterns at running speed <10 cm/s, including a variety of behavioral states such as rearing and brief stops, were classified as slow behavior and excluded from the main analyses. In each motif, a goal-oriented moving direction relative to individual goal ports (angle), a distance between the last point of the motif and the goal ports (distance), and a gap from the nearest lines between individual goal ports and the other ports (gap) were computed (Figures 4A and S5A), which yielded a twelve-dimensional vector. The vectors were then decomposed into two-dimensional vectors by t-distributed stochastic neighbor embedding (t-SNE), a machine learning algorithm (van der Maaten and Hinton, 2008), as shown in Figure 4B. A motif was classified as pGoal-directed behavior (Figure 4B, colored triangles) based on its plot location relative to the other plots obtained from the cued task (Figure 4B, colored circles; for more detail, see STAR Methods and Figure S5B). The other motifs in the pRF task were classified as non-pGoal-directed behavior (Figure 4B, gray triangles). The animals' trajectories and running speed of pGoal-directed behavior are shown in Figures 4C and 4D, respectively (other examples are shown in Figure S5C). Overall, the total periods of pGoal-directed behavior and non-pGoal-directed behavior were 48.3 ± 21.1 s and 136.0 ± 42.5 s (n = 11 rats), respectively, during an entire 600-s period of the pRF task. Spatial distributions of pGoal-directed behavior and non-pGoal-directed behavior are shown in Figure S5D and S5E.

Spatial Firing of Goal-Directed Cells in the pRF Task

We tested the idea that place cells shift their place fields when animals change behavior patterns in response to different task demands (Markus et al., 1995; Smith and Mizumori, 2006; Ferbinteanu et al., 2011) by analyzing spatial firing patterns in different behavioral patterns: the cued task, pGoal-directed behavior, and non-pGoal-directed behavior. An example goal-directed cell (rat 31, cell 1) shown in Figure 4E retained its place field at the same location, irrespective of these behavioral patterns. To quantify the stability of place fields across different behavioral patterns, spatial correlation coefficients were computed between two firing-rate maps (Figure 4F). Out of 37 goal-directed spatial cells tested, 18 cells (48.6%) had significant positive spatial correlations in both the comparison between the cued task and pGoal-directed behavior and the comparison between the cued task and non-pGoal-directed behavior (Figure 4G), which demonstrated that these cells did not remap their fields across the three behavioral patterns. In Figure 5, these non-remapped goal-directed cells were selectively analyzed (n = 18 cells).

For each cell, the animal's goal-oriented moving directions were computed in reference to its goal port identified in the cued task (Figure 5A), and MVL_{goal} was computed from polar plots constructed from firing rates within place fields based on goal-oriented moving directions (Figure 5B). Overall, the behaviors associated with the MVL_{goal} at 0° from high to low were as follows: the cued task, pGoal-directed behavior in the pRF task, and non-pGoal-directed behavior in the pRF task (cued task versus pGoal-directed behavior, $t_{17} = 4.01$, $p = 1.8 \times 10^{-3}$; pGoal-directed behavior

(G) Distributions of spatial correlation coefficients between the cued task and pGoal-directed behavior (left) or between the cued task and non-pGoal-directed behavior (right). Black and gray bars represent significant and non-significant positive spatial correlations, considered as non-remapped and remapped cells, respectively.
See also Figure S5.

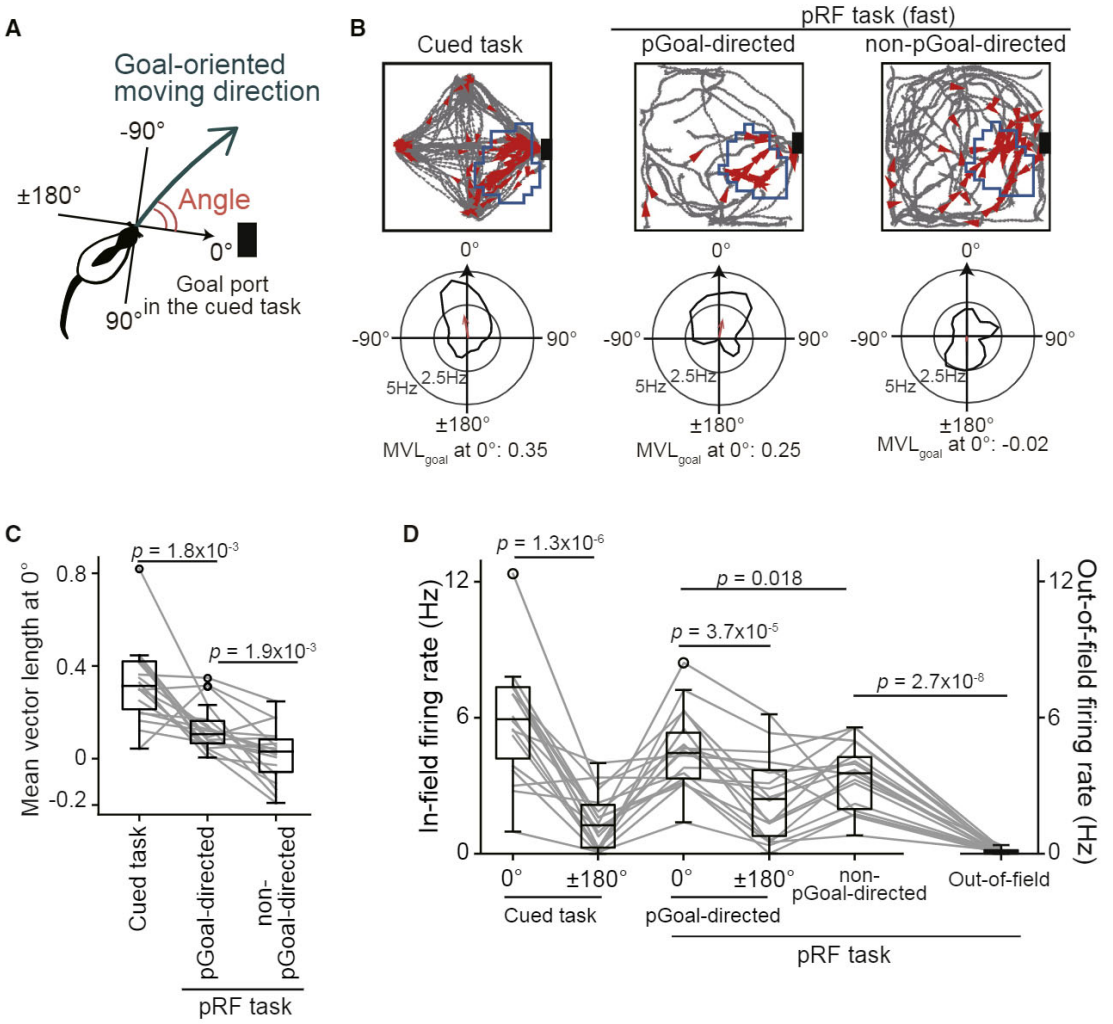

Figure 5. Similar Goal-Directed Firing Appears during pGoal-Directed Behavior in the pRF Task

(A) For each cell, the goal-oriented moving direction relative to a goal port defined in the cued task was computed at each frame. The angles of 0° and ±180° represent running directions toward and away from the goal port, respectively.

(B) Firing patterns of a representative cell in the cued task (left) and during pGoal-directed behavior (middle) and non-pGoal-directed behavior (right) in the pRF task. (Top) Spike locations (red dots) superimposed on animal trajectories (gray line). Place fields defined in individual maps are enclosed by blue lines. The location of the goal port defined in the cued task is shown by black boxes. (Bottom) Polar plots of firing rates as a function of goal-oriented moving direction. In each plot, a mean vector in a polar plot was computed as shown by red arrows.

(C) Comparison of mean vector length at 0° computed based on polar plots as in (B). Paired t test followed by Bonferroni correction.

(D) In-field firing rates at goal-oriented moving directions of 0° and ± 180°. For comparison, in-field firing rates during non-pGoal-directed behavior and out-of-field firing rates are shown in the same graph. Each line shows each cell. Paired t test followed by Bonferroni correction.

versus non-pGoal-directed behavior, $t_{17} = 3.99$, $p = 1.9 \times 10^{-3}$). In-field firing rates in the goal-oriented moving direction at 0° were significantly higher than those at ± 180° (Figure 5D), both in the cued task and during pGoal-directed behavior in the pRF task (cued task, $t_{17} = 7.26$, $p = 1.3 \times 10^{-6}$; pGoal-directed behavior, $t_{17} = 5.52$, $p = 3.7 \times 10^{-5}$). In addition, in-field firing rates at a moving direction of 0° during pGoal-directed behavior were also significantly higher than those during non-pGoal-directed behavior in the pRF task ($t_{17} = 2.63$, $p = 0.018$). Nonetheless, in-field firing rates during non-pGoal-directed behavior were significantly higher than out-of-field firing rates ($t_{17} = 9.63$, $p = 2.7 \times 10^{-8}$) in the pRF task, the same as in the cued task (Figure 3E). These results imply that (1) constant baseline excitatory drives are present for place cells within their place fields, irrespective of goal-directed signals, and (2) in-field firing can be enhanced by internally motivated behavior without specific reward-related cues, as well as visually guided goal-directed behavior.

Medial Septal Inactivation Reduces Goal-Directed Firing and Spatial Firing

We next quantified theta phase precession, in which hippocampal place cells fire at progressively earlier phases of local field

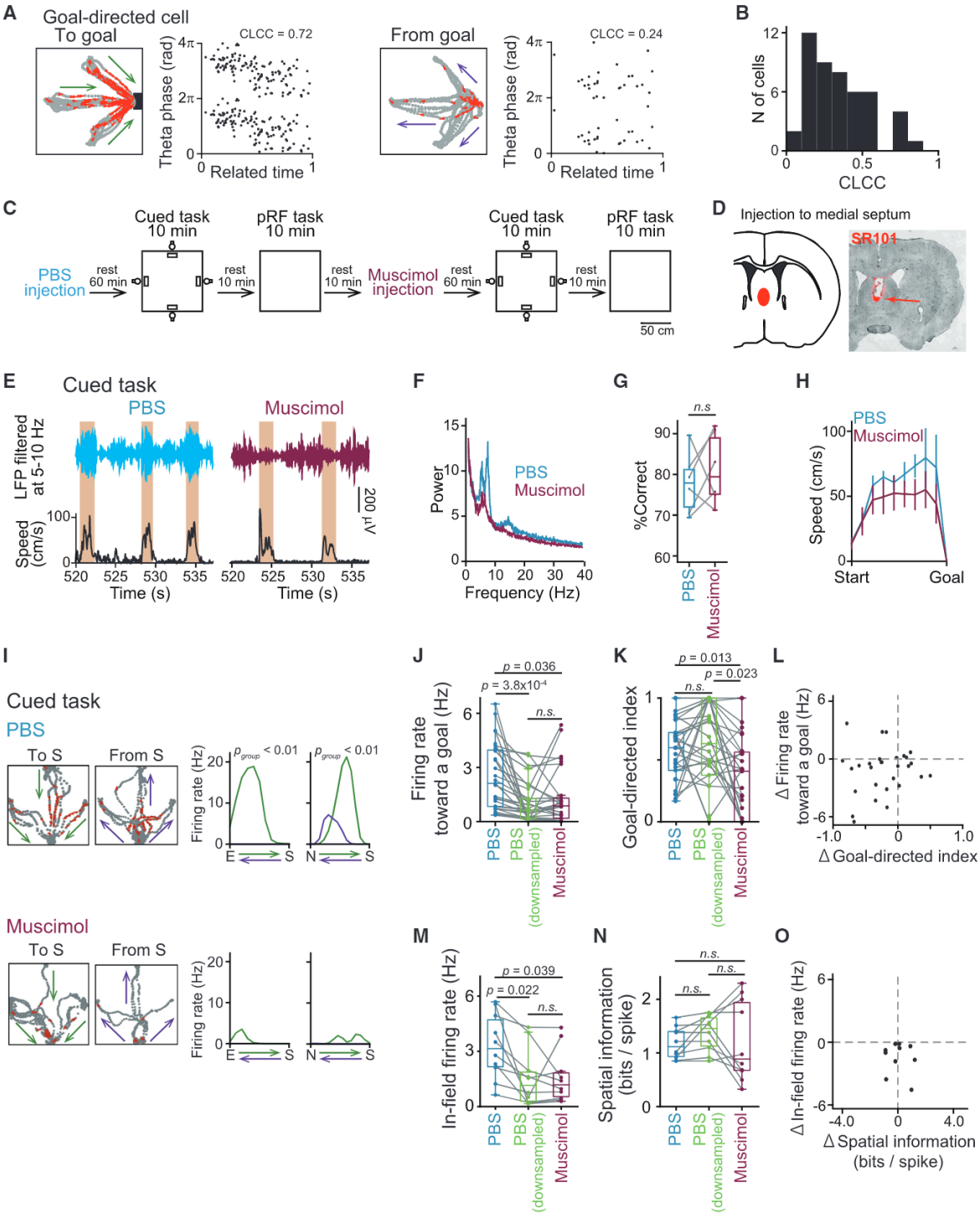

Figure 6. Effects of Theta Power Reduction by Medial Septum Inactivation on Goal-Directed Firing

(A) Theta phase precession of spikes in a representative goal-directed cell in the cued task. The left graphs show spike locations (red dots) superimposed on all trajectories toward the goal port defined for this cell (black box) used for phase precession analysis. The right graphs show the phase-position relationship of the observed spikes. A circular linear correlation coefficient (CLCC) computed from each graph is shown above.

(B) Distribution of CLCCs of all goal-directed cells.

(C) A schematic illustration of experimental paradigms including PBS and muscimol injection into the medial septum.

(D) Histological verification of an injection site labeled with sulforhodamine (SR101) in a coronal brain section. The arrow indicates the tip of an injection cannula.

(legend continued on next page)

potential (LFP) theta cycles (O'Keefe and Recce, 1993; Skaggs et al., 1996; Jeewajee et al., 2013; Schlesiger et al., 2015). For each goal-directed cell, a circular linear correlation coefficient (CLCC) during the cued task was computed between the time spent within the place field and the theta phase of spikes (Figure 6A). The majority (65%) of goal-directed cells showed significant CLCCs with $p < 0.05$, a physiological sign of clear theta phase precession (Figure 6B). The results from the phase precession analysis suggest that goal-directed firing is mediated by theta-associated signals that mainly arise from the medial septum. To test this idea, medial septal activity was inhibited by local infusion of a γ-aminobutyric acid $(GABA)_A$ receptor agonist muscimol into the medial septum (Figures 6C, 6D, and S6A). Inactivation of the medial septum prominently attenuated hippocampal LFP theta power (Figure 6E and 6F) during running in the cued task, but the behavioral performance and running speed remained unchanged (n = 6 rats; Figure 6G; $t_5 = 0.763$, $p = 0.48$; Figure 6H; $F_{1,9} = 1.97$, $p = 0.066$, repeated-measures ANOVA). Overall, medial septum inactivation decreased firing rates of hippocampal cells recorded during the cued task by 36% ± 21% (n = 78 cells; Figures S6A and S6B). The firing patterns of a representative goal-directed cell in the cued task are shown in Figure 6I (other example cells are shown in Figures S6C and S6D). This cell showed a pronounced reduction in firing rates by medial septum inactivation during goal-directed running on significant journeys (NW and EW journeys). Overall, absolute firing rates toward their goal ports and goal-directed indexes of goal-directed cells were significantly decreased by muscimol injection (Figures 6J and 6K; firing rates, $t_{28} = 2.68$, $p = 0.036$; goal-directed indexes, $t_{28} = 2.96$, $p = 0.013$, paired t test followed by Bonferroni correction). While we found a minority of cells increased the goal-directed indexes after muscimol administration (Figure 6K), most of these cells showed a reduction in absolute firing rates as shown in the fourth quadrant in Figure 6L, meaning that the overall strength of goal-directed coding of these cells was not drastically increased by muscimol injection. Absolute in-field firing rates of goal-directed spatial cells were significantly decreased by muscimol injection (Figure 6M; $t_9 = 3.08$, $p = 0.039$, paired t test followed by Bonferroni correction), whereas their spatial information was not significantly changed (Figure 6N; $t_9 = 0.14$, $p > 0.99$, paired t test followed by Bonferroni correction). To test the effects of a reduction in overall firing rates by muscimol injection on goal-directed and spatial coding, spikes were downsampled from the data of the PBS condition so that overall firing rates of individual cells in the PBS condition were similar to those in the muscimol condition, termed PBS-downsampled data. To retain sufficient spike counts, only cells with a total number of spikes greater than 100 were used for this analysis. The PBS-downsampled data showed no significant differences in their goal-directed index (Figure 6K; $t_{28} = 0.32$, $p > 0.99$, paired t test followed by Bonferroni correction) and spatial information (Figure 6N; $t_9 = 2.25$, $p = 0.15$, paired t test followed by Bonferroni correction), compared with the PBS group. These results suggest that the reductions in the overall firing rates by muscimol injection alone cannot account for changes in both goal-directed coding and spatial coding. Similar to the PBS group, the PBS-downsampled data showed a significant difference in the goal-directed index (Figure 6K; $t_{28} = 2.77$, $p = 0.023$, paired t test followed by Bonferroni correction) and a non-significant difference in the spatial information (Figure 6N; $t_9 = 0.86$, $p > 0.99$, paired t test followed by Bonferroni correction), compared with the muscimol group.

Consistent with these results, in the pRF task, inactivation of the medial septum reduced the overall firing rates (Figures S6G and S6H) and the amplification level of in-field firing during pGoal-directed behavior to the level during non-pGoal-directed behavior (Figures S6I and S6J), while it did not significantly alter the running speed and the duration of pGoal-directed behavior (Figures S6E and S6F). Taking all of these results together, medial septal inactivation specifically reduces goal-directed firing of hippocampal cells without inducing pronounced changes in their spatial selectivity.

DISCUSSION

In this study, we systematically analyzed firing patterns of hippocampal CA1 cells recorded from rats performing a series of two tasks, a cued task and a pRF task, in identical open fields. The major findings were that (1) in-field firing rates of hippocampal cells, irrespective of the positional relationship between their place fields and goal locations, were pronouncedly increased when rats were running toward a goal location; (2) in-field firing rates were higher than out-of-field firing rates irrespective of running speed and goal-related directions; (3) pGoal-directed behavior, possibly driven by spontaneous recall of previous spatial memory, induced similar increases in in-field firing rates as goal-directed behavior; and (4) medial septal inactivation

(E) Bandpass-filtered (5–10 Hz) local field potential (LFP) traces and running speed after medial septal injection of PBS (left) and muscimol (right) in the cued task. Running periods toward goal ports are shown in shaded areas.
(F) Fourier transforms power spectra for PBS and muscimol injection into the medial septum.
(G) No difference in the percentages of correct trajectories in the cued task.
(H) Averaged time changes in running speed from a reward port to the next one after PBS and muscimol administration, as shown in Figure 1F (n = 530 trajectories from four animals).
(I) Firing patterns of a representative goal-directed cell after PBS and muscimol administration in the cued task, shown as in Figure 2A. For simplification, only significant journeys are presented.
(J, K, M, and N) Comparison of goal-directed firing rates (J), goal-directed index (K), in-field firing rates (M), and spatial information (N) between PBS and muscimol administration in the cued task. Paired t test followed by Bonferroni correction.
(L) Plotting differences in goal-directed index and goal-directed firing rates by muscimol administration, from the same datasets as in (J) and (K). Each dot shows each cell.
(O) Plotting differences in spatial information and in-field firing rates by muscimol administration, from the same datasets as in (M) and (N).
See also Figure S6.

reduced goal-directed firing rates, while spatial representation patterns were normally retained.

This study examined goal-directed firing at a running speed >10 cm/s, which is different from reported firing patterns observed when animals wait at a specific goal location (Hok et al., 2007). The proportion of goal-directed cells found in our cued task was 15.8%. Compared with this proportion, the bat hippocampus showing vectorial representations in a three-dimensional space had a nearly similar proportion of goal-directed cells (18.8%) (Sarel et al., 2017). These results suggest that both rats and flying bats might utilize similar mechanisms for hippocampal neuronal populations to encode goal-directed information. A recent study by Grieves et al. (2016) has suggested that place cell firing is mainly determined by an animal's routes rather than destinations. In the spatial task by Grieves et al. (2016), rats need to pass through two choice points to reach the final goal from place fields analyzed, whereas rats simply run through a simple straight path for an immediate goal in our spatial task. The difference in task conditions suggests that the meaning of the final destination for rats may be considerably different between the two tasks. If the goal-directed firing tested in our study is regarded as a representation of an immediate future trajectory, our result is consistent with the claim by Grieves et al. (2016) that place cells encode immediate future routes rather than destinations.

Trajectory-dependent firing of hippocampal place cells has been reported from spatial tasks with left/right choices on linear paths (Wood et al., 2000; Ferbinteanu and Shapiro, 2003; Ainge et al., 2007; Ji and Wilson, 2007; Catanese et al., 2014; Ito et al., 2015; Grieves et al., 2016). In addition to the growing body of evidence, our results suggests that (1) in-field firing-rate increases occur when animals pass through the place fields from any directions toward a specific goal in a two-dimensional space and (2) the trajectory-dependent in-field firing increases are diminished during moving in the opposite directions. It is likely a general characteristic of place cells that spatial firing is amplified by goal-directed behavior, which may comprehensively account for the trajectory-dependent firing reported in the previous studies.

Our data suggest possible neurophysiological mechanisms for combing place-selective and goal-directed signals within a hippocampal cell. First, some cell populations had place fields distant from goal locations, so-called distant fields, demonstrating that these cells can represent two independent pieces of information using two different encoding modes: (1) spatial representation by increasing firing rates within place fields and (2) goal-directed representation by increasing the in-field firing rates specifically while the animal is moving toward a goal location. Second, the observations that in-field firing rates were not completely zero during any behavioral periods, such as non-pGoal-directed behavior, and were higher than out-of-field firing rates suggest that there are likely substantial place-selective excitatory drives that sustain minimum in-field firing rates in hippocampal place cells. Such firing activity may serve to construct a basal spatial map to purely represent external space independent of goal-directed signals. Third, the observations that in-field firing rates were specifically increased when the animal ran toward goal locations suggest that goal-directed signals may serve to amplify place-selective signals to be integrated upon the basal spatial map. The results that place cells can transiently boost in-field firing rates when animals occasionally exhibit internally generated pGoal-directed behavior suggest that ongoing changes in an animal's internal states (possibly motivation and attention) might account for the trial-to-trial variability of in-field firing of place cells (Fenton and Muller, 1998; Fenton et al., 2010; Yagi et al., 2018).

Goal-directed signals are likely associated with attention, expectation of reward, and motivation. Such higher-order information processing is mediated not only within the hippocampal circuit but also by the complex integration of the extended circuitry outside of the hippocampus. We demonstrated that goal-directed firing undergoes theta phase precession, a phenomenon mediated by inputs from the medial entorhinal cortex (Schlesiger et al., 2015). Medial septal inactivation reduced the goal-directed index and absolute frequencies of both goal-directed and spatial firing, while it did not change the goal-directed behavior and running speed in either the pRF task or the cued task. These results show that the hippocampus encodes goal-directed signals but such neuronal encoding did not directly affect simple behavioral patterns in our task condition. In addition, medial septal inactivation did not impair the spatial encoding, consistent with previous reports (Koenig et al., 2011; Brandon et al., 2014), meaning that the spatial encoding of hippocampal cells was unchanged. These results suggest that the major roles of the medial septal inputs to the hippocampus are not to construct spatial representations but to amplify goal-directed firing during appropriate periods. Given that neuronal processing is determined by the selectivity and intensity of encoding, our results suggest that the medial septum is crucial for processing both goal-directed and spatial information by hippocampal cells.

Recent work has shown that a place cell not only represents space but also exhibits different nonspatial and contextual signals (Aronov et al., 2017). Goal-directed firing in conjunction with spatial representation has been suggested to play a crucial role in not simply representing external space but also flexibly navigating animals to target locations (Gerstner and Abbott, 1997). The flexible combination of these signals may enhance the capacity of the hippocampal network to provide proper signals to spatial navigation modules in the brain and may form the basis of hippocampus-dependent episodic memory.

STAR★METHODS

Detailed methods are provided in the online version of this paper and include the following:

- KEY RESOURCES TABLE
- CONTACT FOR REAGENT AND RESOURCE SHARING
- EXPERIMENTAL MODEL AND SUBJECT DETAILS
- METHOD DETAILS
  - The Cued Task
  - A Pseudorandom Foraging (pRF) Task
  - Surgical Procedures
  - Monitoring Animal's Locations and Head Directions
  - Adjusting Electrode Depth

SUPPLEMENTAL INFORMATION

Supplemental Information can be found online at https://doi.org/10.1016/j.celrep.2019.04.002.

ACKNOWLEDGMENTS

This work was supported by Kaken-hi (17H05551 and 17H05939), the JST-ERATO program (JPMJER1801), the Takeda Science Foundation, and the Precursory Research for Embryonic Science and Technology program (JPMJPR1785).

AUTHOR CONTRIBUTIONS

Y.A. and T.S. designed the study. Y.A. and H.I. performed the surgery and set up the experimental apparatus. Y.A. acquired the electrophysiological data and Y.A. and H.I. performed the analysis. Y.I. supervised the project. Y.A. and T.S. prepared all of the figures. T.S. wrote the main manuscript text and all authors reviewed the main manuscript text.

DECLARATION OF INTERESTS

The authors declare no competing interests.

Received: October 8, 2018
Revised: February 17, 2019
Accepted: March 27, 2019
Published: April 30, 2019

REFERENCES

Aghajan, Z.M., Acharya, L., Moore, J.J., Cushman, J.D., Vuong, C., and Mehta, M.R. (2015). Impaired spatial selectivity and intact phase precession in two-dimensional virtual reality. Nat. Neurosci. *18*, 121–128.

Ainge, J.A., Tamosiunaite, M., Woergoetter, F., and Dudchenko, P.A. (2007). Hippocampal CA1 place cells encode intended destination on a maze with multiple choice points. J. Neurosci. *27*, 9769–9779.

Aronov, D., Nevers, R., and Tank, D.W. (2017). Mapping of a non-spatial dimension by the hippocampal-entorhinal circuit. Nature *543*, 719–722.

Brandon, M.P., Koenig, J., Leutgeb, J.K., and Leutgeb, S. (2014). New and distinct hippocampal place codes are generated in a new environment during septal inactivation. Neuron *82*, 789–796.

Catanese, J., Viggiano, A., Cerasti, E., Zugaro, M.B., and Wiener, S.I. (2014). Retrospectively and prospectively modulated hippocampal place responses are differentially distributed along a common path in a continuous T-maze. J. Neurosci. *34*, 13163–13169.

Fenton, A.A., and Muller, R.U. (1998). Place cell discharge is extremely variable during individual passes of the rat through the firing field. Proc. Natl. Acad. Sci. USA *95*, 3182–3187.

Fenton, A.A., Lytton, W.W., Barry, J.M., Lenck-Santini, P.P., Zinyuk, L.E., Kubík, S., Bures, J., Poucet, B., Muller, R.U., and Olypher, A.V. (2010). Attention-like modulation of hippocampus place cell discharge. J. Neurosci. *30*, 4613–4625.

Ferbinteanu, J., and Shapiro, M.L. (2003). Prospective and retrospective memory coding in the hippocampus. Neuron *40*, 1227–1239.

Ferbinteanu, J., Shirvalkar, P., and Shapiro, M.L. (2011). Memory modulates journey-dependent coding in the rat hippocampus. J. Neurosci. *31*, 9135–9146.

Frank, L.M., Brown, E.N., and Wilson, M. (2000). Trajectory encoding in the hippocampus and entorhinal cortex. Neuron *27*, 169–178.

Gauthier, J.L., and Tank, D.W. (2018). A dedicated population for reward coding in the hippocampus. Neuron *99*, 179–193.e177.

Gerstner, W., and Abbott, L.F. (1997). Learning navigational maps through potentiation and modulation of hippocampal place cells. J. Comput. Neurosci. *4*, 79–94.

Grieves, R.M., Wood, E.R., and Dudchenko, P.A. (2016). Place cells on a maze encode routes rather than destinations. eLife *5*, e15986.

Hardcastle, K., Maheswaranathan, N., Ganguli, S., and Giocomo, L.M. (2017). A multiplexed, heterogeneous, and adaptive code for navigation in medial entorhinal cortex. Neuron *94*, 375–387.e377.

Hok, V., Lenck-Santini, P.P., Roux, S., Save, E., Muller, R.U., and Poucet, B. (2007). Goal-related activity in hippocampal place cells. J. Neurosci. *27*, 472–482.

Ito, H.T., Zhang, S.J., Witter, M.P., Moser, E.I., and Moser, M.B. (2015). A prefrontal-thalamo-hippocampal circuit for goal-directed spatial navigation. Nature *522*, 50–55.

Jackson, J., and Redish, A.D. (2007). Network dynamics of hippocampal cell-assemblies resemble multiple spatial maps within single tasks. Hippocampus *17*, 1209–1229.

Jeewajee, A., Barry, C., Douchamps, V., Manson, D., Lever, C., and Burgess, N. (2013). Theta phase precession of grid and place cell firing in open environments. Philos. Trans. R. Soc. Lond. B Biol. Sci. *369*, 20120532.

Ji, D., and Wilson, M.A. (2007). Coordinated memory replay in the visual cortex and hippocampus during sleep. Nat. Neurosci. *10*, 100–107.

Koenig, J., Linder, A.N., Leutgeb, J.K., and Leutgeb, S. (2011). The spatial periodicity of grid cells is not sustained during reduced theta oscillations. Science *332*, 592–595.

Markus, E.J., Qin, Y.L., Leonard, B., Skaggs, W.E., McNaughton, B.L., and Barnes, C.A. (1995). Interactions between location and task affect the spatial and directional firing of hippocampal neurons. J. Neurosci. *15*, 7079–7094.

McNaughton, B.L., Barnes, C.A., and O'Keefe, J. (1983). The contributions of position, direction, and velocity to single unit activity in the hippocampus of freely-moving rats. Exp. Brain Res. *52*, 41–49.

Muller, R.U., Bostock, E., Taube, J.S., and Kubie, J.L. (1994). On the directional firing properties of hippocampal place cells. J. Neurosci. *14*, 7235–7251.

O'Keefe, J., and Dostrovsky, J. (1971). The hippocampus as a spatial map. Preliminary evidence from unit activity in the freely-moving rat. Brain Res. *34*, 171–175.

O'Keefe, J., and Nadel, L. (1978). The Hippocampus as a Cognitive Map (Oxford University Press).

O'Keefe, J., and Recce, M.L. (1993). Phase relationship between hippocampal place units and the EEG theta rhythm. Hippocampus *3*, 317–330.

Redish, A.D. (2009). MClust 3.5, Free-Ware Spike Sorting. (University of Minnesota). http://redishlab.neuroscience.umn.edu/MClust/MClust.html.

Sarel, A., Finkelstein, A., Las, L., and Ulanovsky, N. (2017). Vectorial representation of spatial goals in the hippocampus of bats. Science *355*, 176–180.

Schlesiger, M.I., Cannova, C.C., Boublil, B.L., Hales, J.B., Mankin, E.A., Brandon, M.P., Leutgeb, J.K., Leibold, C., and Leutgeb, S. (2015). The medial entorhinal cortex is necessary for temporal organization of hippocampal neuronal activity. Nat. Neurosci. *18*, 1123–1132.

Schmitzer-Torbert, N., Jackson, J., Henze, D., Harris, K., and Redish, A.D. (2005). Quantitative measures of cluster quality for use in extracellular recordings. Neuroscience *131*, 1–11.

Skaggs, W.E., McNaughton, B.L., Wilson, M.A., and Barnes, C.A. (1996). Theta phase precession in hippocampal neuronal populations and the compression of temporal sequences. Hippocampus *6*, 149–172.

Smith, D.M., and Mizumori, S.J. (2006). Learning-related development of context-specific neuronal responses to places and events: the hippocampal role in context processing. J. Neurosci. *26*, 3154–3163.

Takahashi, S. (2015). Episodic-like memory trace in awake replay of hippocampal place cell activity sequences. eLife *4*, e08105.

Taube, J.S., Muller, R.U., and Ranck, J.B., Jr. (1990). Head-direction cells recorded from the postsubiculum in freely moving rats. I. Description and quantitative analysis. J. Neurosci. *10*, 420–435.

van der Maaten, L., and Hinton, G. (2008). Visualizing data using t-SNE. J. Mach. Learn. Res. *9*, 2579–2605.

Wood, E.R., Dudchenko, P.A., Robitsek, R.J., and Eichenbaum, H. (2000). Hippocampal neurons encode information about different types of memory episodes occurring in the same location. Neuron *27*, 623–633.

Yagi, S., Igata, H., Shikano, Y., Aoki, Y., Sasaki, T., and Ikegaya, Y. (2018). Time-varying synchronous cell ensembles during consummatory periods correlate with variable numbers of place cell spikes. Hippocampus *28*, 471–483.

STAR★METHODS

KEY RESOURCES TABLE

REAGENT or RESOURCE	SOURCE	IDENTIFIER
Chemicals, Peptides, and Recombinant Proteins		
Isoflurane	Zoetis	Cat#6073253
Muscimol	Sigma-Aldrich	Cat#057M4010V
Praformaldehyde	Nacalai tesque	Cat#M8E4590
Cresyl violet	Sigma-Aldrich	Cat#125K3707
Re-fine Bright	Yamahachi Dental Mfg., Co.	Cat#KH01
Hydrogen Hexachloroplatinate(IV) Hexahydrate	Nacalai tesque	Cat#V8P4386
Experimental Models: Organisms/Strains		
Long Evans rats	SLC	http://www.jslc.co.jp/animals/rat.php
Software and Algorithms		
	MathWorks	https://jp.mathworks.com/
MClust	A.D. Redish	http://redishlab.neuroscience.umn.edu/MClust/MClust.html
LN model MATLAB codes	Giocomo Lab; Hardcastle et al., 2017	https://github.com/GiocomoLab/ln-model-of-mec-neurons/
Circular Statistics Toolbox	Philipp Berens	https://jp.mathworks.com/matlabcentral/fileexchange/10676-circular-statistics-toolbox-directional-statistics
Python 2.7	Python Software Foundation	https://www.python.org/about/
Other		
Micro syringe	Ito	Model: MS-E05
Syringe pump	Muromachi	Model: Legato 100
Cannula	Eicom	Model: AC-5, AG-12, AD-12
Microtome	Leica	Model: SM2010 R
Platinum-Iridium tetrode wire	California Fine Wire Company	Cat#CFW0011173
Neural signal processor	BLACKROCK	Model: Cerebus
Microdrive	Custom built	N/A

CONTACT FOR REAGENT AND RESOURCE SHARING

Further information and requests for resources and reagents should be directed to and will be fulfilled by the Lead Contact, Takuya Sasaki (tsasaki@mol.f.u-tokyo.ac.jp).

EXPERIMENTAL MODEL AND SUBJECT DETAILS

All experiments were performed with the approval of the experimental animal ethics committee at the University of Tokyo (approval number: P29-11) and according to the NIH guidelines for the care and use of animals.

A total of 11 male Long Evans rats (2-5 months old) with a preoperative weight of 290–440 g were used in this study. The animals were housed individually and maintained on a 12-h light/12-h dark schedule with lights off at 7:00 AM. All animals were purchased from SLC (Shizuoka, Japan). Following at least 1 week of adaptation to the laboratory, the rats were reduced to 85% of their *ad libitum* weight through limited daily feeding. Water was readily available.

METHOD DETAILS

The Cued Task

Before surgery, the rats were trained to perform a cued spatial task on a 100-cm-sided square open field (elevated 75 cm from the floor) with a wall height of 40 cm. All behavioral experiments occurred in the dark phase. On the first 2 days, the rats were habituated to the open field by allowing them to freely forage for randomly scattered chocolate milk for 10 min. After the habituation period, the animals were trained to perform a cued task in which they learned the association between illuminated cue lights and reward

availability so that they continuously ran from a reward port to the next port (training phase). Here, four reward ports (4 × 5 cm) were placed on the field in the middle of individual walls, and downward-facing white light-emitting diodes (LEDs) were attached to the walls 12 cm above the individual reward ports, as shown in Figure 1A. When a cue light was illuminated, the corresponding reward port dispensed 0.2 mL of chocolate milk reward by a syringe pump. The detected signals were digitized and timestamped by a laptop computer. On a single training day, the rat was first placed in the center of the field, and a randomly chosen cue light was illuminated, indicating that the corresponding reward port provided chocolate milk reward. Once the animal reached the port and started to consume the reward, a custom-made photosensor attached to the reward port detected the animal's head, which then triggered the extinction of the current light cue and the illumination of the other randomly chosen cue light, coinciding with the delivery of a new reward underneath the illuminated light. The cue position was pseudorandom, and the identical port was not rewarded successively. On a single training day, this procedure was repeated as much as possible in a 10-min session. Because reward supply and cue presentation were controlled by a computer, it was not necessary to handle the rat once a training session began. This training was repeated daily for 10 min until the animal learned the task and was able to consume the reward from at least 40 correct trajectories within the 10-min period. To achieve this criterion performance, training lasted 5-15 days. The rats were kept in a rest box (30 × 30 cm) outside the field for tens of minutes before and after the task.

A Pseudorandom Foraging (pRF) Task

After performing the cued task, the animal was allowed to rest for 10 min, during which the floor of the field was cleaned with water, and all four reward ports were removed from the field. The animal was then placed in the same field and allowed to freely forage for randomly scattered chocolate milk for 10 min. For at least three days before recording days, the animals were trained to perform this random foraging behavior after cued task training on training days. These animals occasionally exhibited pseudo-goal-directed behavior (pGoal-directed behavior; see Figures 4C and S5C), and this foraging task was thus termed a pRF task.

Surgical Procedures

The rat was anesthetized with isoflurane gas (1%–2.5%). A craniotomy with a diameter of ~2 mm was performed using a high-speed drill, and the dura was surgically removed. Two stainless-steel screws were implanted in the bone above the frontal cortex to serve as ground and reference electrodes. An electrode assembly that consisted of 8–16 independently movable tetrodes, which was created using a 3D printer (Form 2, Formlabs), was stereotaxically implanted above the right hippocampus (4.0 mm posterior and 2.7 mm lateral to bregma). The tip of the electrode bundle was lowered to the cortical surface, and the electrodes were inserted 1.25 mm into the brain at the end of surgery. The electrodes were constructed from 17-μm-wide polyimide-coated platinum-iridium (90/10%) wire (California Fine Wire), and the electrode tips were plated with platinum to lower electrode impedances to 150–300 kΩ at 1 kHz.

In addition to the tetrode assembly, four rats underwent surgery for implanting a guide tube (inner diameter = 0.34 mm and outer diameter = 0.5 mm, AG-12, Eicom, Japan) at an angle of 30° in the sagittal plane and 15° in the coronal plane into the medial septum (3.3 mm anterior and 1.9 mm lateral to bregma, and 6.6 mm inserted into the tissue). The recording device was secured to the skull using stainless-steel screws and dental cement (Re-fine Bright, Yamahachi dental MFG., Co.). Following surgery, each rat was housed individually in transparent Plexiglass with free access to water and food for at least 3 days and was then food deprived to 85% of their body weight. To prevent drying in the guide tube, a dummy plastic cannula with a diameter of 0.33 mm was inserted into the guide tube until the muscimol injection described below.

Monitoring Animal's Locations and Head Directions

To monitor the rat's moment-to-moment position, three red LEDs with a dimeter of 5 mm were attached to the electrode assembly in an isosceles triangle shape (base = 3 cm, legs = 4 cm) with the vertex oriented toward animal's head direction. The position of the vertex of the LED signal was tracked at 25 Hz using a video camera attached to the ceiling. In addition, a head direction at each frame was computed as a direction from the middle point of the base to the vertex in the three LED positions.

Adjusting Electrode Depth

The rat was connected to the recording equipment via Cereplex M (Blackrock), a digitally programmable amplifier, close to the rat's head. The output of the headstage was conducted via a lightweight multiwire tether and a commutator to the Cerebus recording system (Blackrock), a data acquisition system. Electrode turning was performed while the rat was resting in a pot placed on a pedestal. Over a period of at least 2 weeks after surgery, electrode tips were advanced slowly 25–100 μm per day for 14–21 days until spiking cells were encountered in the CA1 layer of the hippocampus, which was identified on the basis of local field potential (LFP) signals and single-unit spike patterns. Once the tetrodes were adjacent to the cell layer, as indicated by the presence of low-amplitude multiunit activity, tetrodes were settled into the cell layer for stable recordings over a period of several days.

Electrophysiological Recording

Recording began after stable well-separated unit activity was identified in the hippocampus. The behavioral paradigm after surgery was identical to the training performed prior to surgery. Before the recording was begun, the animals were trained daily for up to 14 days. In some cases, the training was performed with the recording headstage and cable attached so that the animals became

familiar with the recording condition. After confirmation that the animals again reached criterion performance (80% correct) in the cued task, as in the presurgery period, electrophysiological data collection commenced in the cued task and the pRF task. LFP recordings were sampled at 2 kHz and filtered between 0.1 and 500 Hz. Unit activity was amplified and bandpass filtered at 500 Hz to 6 kHz. Spike waveforms above a trigger threshold (63 μV) were timestamped and recorded at 30 kHz for 1.6 ms. Recordings were conducted for at least 2 days.

For muscimol injection, the dummy cannula was removed from the guide tube and replaced by a plastic injection cannula with a diameter of 0.34 mm so that the tip of the injection cannula reached above the medial septum. The other side of the injection cannula was connected by polyethylene tubing to a 5 μL syringe mounted in an infusion pump (KDS LEGATO101, Muromachi, Japan). Through the injection cannula, 0.5 μg/μl muscimol dissolved in phosphate-buffered saline (PBS; pH 7.4) was then infused for 4 min into the medial septum at a rate of 0.25 μl/min. After the infusions were completed, the injection cannula was left in place for 30 min, and the animals were placed back in the rest box for 1 hour. Then, the dummy cannula was again inserted into the guide tube. The spatial distribution of muscimol was estimated by infusion of 0.5 μg/μl sulforhodamine (SR101) (Invitrogen) in PBS at a rate of 0.25 μl/mi for 4 min (Figure 6D). During the muscimol injection procedure, the animals did not show any sign of stress or discomfort.

Histological Analysis to Confirm Electrode Placement

The rats received an overdose of urethane, were intracardially perfused with 4% paraformaldehyde in PBS and decapitated. To aid the reconstruction of electrode tracks, the electrodes were not withdrawn from the brain until 8–12 hours after perfusion. After dissection, the brains were fixed overnight in 4% paraformaldehyde (PFA) and then equilibrated with a sequence of 20% sucrose and 30% sucrose in PBS. Frozen coronal sections (50 μm) were cut using a microtome, and serial sections were mounted and processed for cresyl violet staining. For cresyl violet staining, the slices were rinsed in water, counterstained with cresyl violet, and coverslipped with Permount. The positions of all tetrodes were confirmed by identifying the corresponding electrode tracks in histological tissue. Recordings were included in the data analysis if the tetrode's deepest position was in the cell layer.

QUANTIFICATION AND STATISTICAL ANALYSIS

Spike Sorting

Spike sorting was performed offline using the graphical cluster-cutting software MClust (Redish, 2009). Rest recordings before and after the behavioral paradigms were included in the analysis to assure recording stability throughout the experiment and to identify hippocampal cells that were silent during behavior. Clustering was performed manually in two-dimensional projections of the multi-dimensional parameter space (i.e., comparisons between waveform amplitudes, the peak-to-trough amplitude differences, and waveform energies, each measured on the four channels of each tetrode). Units with spike amplitudes of 100 μV and twice the mean noise were discriminated offline by identifying clusters defined by waveform parameters. The cluster quality was measured by computing the L_{ratio} and isolation distance (Schmitzer-Torbert et al., 2005). A cluster was considered as a cell when the L_{ratio} was less than 0.30 and the isolation distance was more than 14. Autocorrelation and cross-correlation functions were used as additional separation criteria. Refractory periods of spikes were considered to increase confidence in the successful isolation of cells. Cells with an average firing rate of less than 3 Hz were considered to be putative excitatory cells and included in the analysis. To eliminate possible repeated recordings of the same neurons across different days, data from each tetrode were obtained from only one day (which yielded the maximum number of cells).

Analysis of Spike Patterns in the Cued Task

The cued task had twelve ($_4P_2$) possible journey patterns from a reward port to the next port. To evaluate the correctness of individual trajectories, a trajectory of an animal from a previous reward to the next reward was projected onto the straight line between the two reward ports. A trajectory was defined as a correct trajectory if the maximum projection distance to the straight line was less than 20 cm (that is, a trajectory was included within the blue region in Figure 1B). In contrast, a trajectory was defined as an error trajectory if at least one projection distance elsewhere on the trajectory exceeded 20 cm (that is, a trajectory ran over the blue region in Figure 1B).

The following analyses were applied for each cell. Only spikes and locations at a running speed of > 10 cm/s on correct trajectories were used for analyses. For each journey, the animal's coordinates and the positions of neuronal spikes were projected onto the corresponding straight line, and the average firing-rate distribution was computed along the line by dividing the total number of spikes in each location bin (7.5 cm) along the line by the total time that the animal spent in that bin. All firing-rate distributions were smoothed by a one-dimensional convolution with a Gaussian kernel with a standard deviation of one pixel (7.5 cm). For each line, the selectivity of the moving direction was evaluated by computing p_{group} using two-way repeated-measures ANOVA (factors: place and repetition of trajectory), which quantifies the significant difference in firing-rate distributions between two journeys with opposite directions on the line. This ANOVA was not applied to a line if both firing-rate distributions had a maximum firing rate less than 2 Hz (shown by N/A). A journey with a significantly higher firing-rate distribution was considered a significant journey when the p_{group} was less than 0.01. A goal-directed cell was defined as a cell with at least one direction-dependent journey, and a goal port for a goal-directed cell was defined as the reward port with the maximum number of direction-dependent journeys for that cell. Cells with no significant firing-rate distributions were classified as non-goal-directed cells. For each goal-directed cell, a goal-directed index was computed as

the equation shown in Figure 2C, where average firing rates on significant journeys moving toward and from a goal port were used for analysis. For quantifying spatial selectivity, only periods with instantaneous running speeds greater than 10 cm/s were included for analysis. For each cell, a spatial firing-rate distribution was constructed by dividing the sum of the total number of spikes in each location bin (5 cm × 5 cm) by the amount of time that the animal spent in that bin. Data were smoothed with a Gaussian kernel filter with a standard deviation of one pixel (5 cm), constructing a tuning curve map (Figures 3A and 3B, middle). The tuning curve firing-rate map was then compensated by running speed using the linear-nonlinear-Poisson (LN) model (for detail, see Hardcastle et al., 2017) and was termed the LN model map. Based on the LN model map, an information density was computed by the following formula:

$$I = \sum_{i=1}^{N} p_i \frac{r_i}{r} \log_2 \frac{r_i}{r}$$

where I is the information density measured in bits per spike, i is the index of the pixels of the place field, p_i is the probability of the animal being at location i, r_i is the average firing rate of the cell when the animal is at location i, and r is the total average firing rate. A cell was classified as a spatial (place) cell if both of the following criteria were met: (1) the spatial information was more than 0.5, and (2) the spatial information was more than 5% of the top of those computed from 1000 randomized data in which spike times were shifted along the recording period by a random amount between 10 s and the duration of the recording session minus 10 s (Aronov et al., 2017).

Analysis of Spike Patterns in the pRF Task

In the pRF task, behavioral patterns were classified into pGoal-directed behavior, non-pGoal-directed behavior, and slow behavior (Figure 4). Slow behavior was defined as periods with a running speed less than 10 cm/s, whereas individual trajectories in which instantaneous running speed more than 10 cm/s lasting for more than 1 s were termed as moving motifs and subject to following analyses. For each motif both in the cued task and pRF task, a moving angle relative to individual goal ports (corresponding with a goal-oriented moving direction) and a physical distance between the last position of the motif and the port were computed as an "angle" and a "distance." In addition, the average projection distance of moment-to-moment positions included in the motif to the nearest straight line between the goal port and the other port was computed as a "gap" (Figures 4A and S5A). The three factors were computed for four ports, resulting in a twelve-dimensional vector from each motif. All vectors toward specific goal ports in the cued task and pRF task were decomposed into two-dimensional vectors by tSNE (Figures 4B and S5B). For each motif in the pRF task (shown as a triangle), an average plot-plot distance between the motif and the five nearest plots obtained from the cued task (shown as circles) was computed as shown in a distribution of Figure S5B2. A motif in the pRF was classified as pGoal-directed behavior (Figure 4B, colored triangles) if the plot-plot distance was less than (mean + 2 × SD) computed from a standardized normal distribution (orange line) obtained by fitting a histogram below the double of the distance giving the highest peak. This computation was based on an assumption that the smallest unimodal distribution represents a cluster of pGoal-directed behavior. The other motifs were classified as non-pGoal-directed behavior (Figure 4B, gray triangles).

For each cell, the Pearson correlation coefficient was calculated between two spatial maps. Pixels visited less than 150 ms in either session were excluded to avoid artifacts in the correlation measure.

Analysis of Directional Tuning of Spikes

In Figure S3A, for each cell, the head direction tuning curve was computed by plotting the firing rate at a certain range of running speeds as a function of θ, divided into bins of 30° and smoothed with a Gaussian kernel filer with standard deviation of one bin (30°), and a mean vector length (Rayleigh r-value) was calculated as MVL_{head}.

In Figures 5A and S3A, for each point on the animal's trajectories, the angle θ formed by the moving direction at the point and a straight line connecting the point of the animal and the goal port defined in the cued task was calculated, termed a goal-oriented moving direction. An angle $\theta = 0°$ indicates that the animal was moving directly toward the goal port, and $\theta = 180°$ indicates that the animal was moving directly away from the goal port. For each cell, the goal-oriented moving direction tuning curve was computed by plotting the firing rate at a certain range of running speeds as a function of θ, divided into bins of 30° and smoothed with a Gaussian kernel filer with standard deviation of one bin (30°), and a mean vector length (Rayleigh r-value) was calculated as MVL_{goal}.

In Figure S4A, for each point on the animal's trajectories, the angle θ formed by the animal's head direction at the point and a straight line connecting the animal and the goal port defined in the cued task was calculated, termed a goal-oriented head direction. After consuming a reward at a port, the animal oriented the head toward the next goal port, termed goal-oriented behavior. During each goal-oriented behavior, a goal-pointing onset for each goal-directed cell was defined when a goal-oriented head direction first became less than 30° during goal-oriented behavior (an example shown in Figure S4A, right).

Phase Precession Analysis

LFP traces were bandpass filtered at 5 and 10 Hz. Spike timing was normalized so that individual trajectories within place fields were from 0 to 1, defining related time. The quality of phase precession within a place field was defined as the circular linear correlation coefficient (CLCC) between spike phases and the latency of spike timing as described elsewhere (Aghajan et al., 2015).

Statistical Analysis

All data are presented as the mean ± standard error of the mean (SEM) and were analyzed using Python and MATLAB. Comparisons of two-sample data were analyzed by paired t test. Multiple group comparisons of mean firing properties were performed by post hoc Bonferroni corrections. The null hypothesis was rejected at the $p < 0.05$ level.

DATA AND SOFTWARE AVAILABILITY

MClust software is available from A.D. Redish at http://redishlab.neuroscience.umn.edu/MClust/MClust.html. Reasonable requests for data and for software will be fulfilled by the lead contact.